

# Solid-state tellurium-125 nuclear magnetic resonance studies of transition-metal ditellurides <sup>†</sup>

Isabelle Orion,<sup>a</sup> João Rocha,<sup>\*,a</sup> Stéphane Jobic,<sup>b</sup> Virginie Abadie,<sup>b</sup> Raymond Brec,<sup>b</sup> Christian Fernandez<sup>c</sup> and Jean-Paul Amoureaux<sup>c</sup>

<sup>a</sup> Department of Chemistry, University of Aveiro, 3810 Aveiro, Portugal

<sup>b</sup> Laboratoire de Chimie des solides, Institut des Matériaux de Nantes, 2 Rue de la Houssinière, 44072 Nantes Cedex 03, France

<sup>c</sup> Laboratoire de Dynamique et Structure des Matériaux Moléculaires, CNRS URA 801, Université des Sciences et Technologies de Lille, 59655 Villeneuve d'Ascq Cedex, France

Solid-state <sup>125</sup>Te NMR studies of inorganic compounds containing tellurium in oxidation states ranging from -II to VI have been made. The chemical shift tensors of Te(OH)<sub>6</sub>, TeCl<sub>4</sub>, TeO<sub>2</sub> and elemental tellurium have been determined by simulation of magic angle spinning (MAS) NMR spectra. Binary transition-metal ditellurides have been studied by MAS and static <sup>125</sup>Te NMR techniques. The observed MTe<sub>2</sub> NMR shifts range from *ca.* 500 to 8000 ppm [from aqueous Te(OH)<sub>6</sub>] and are shown to be correlated with the expected tellurium oxidation state. Separation of the chemical shift and Knight shift contributions has been attempted.

In the past two decades the synthetic chemistry of transition-metal chalcogenides has developed rapidly, mainly because these compounds display a rich structural chemistry<sup>1</sup> and a wide variety of unusual physical properties inherent to their anisotropic structural arrangement. Until recently the tellurides had received much less attention than the sulfides and the selenides. Nevertheless, the higher electropositive character of tellurium relative to its lighter congeners leads to a greater variability in Te–Te bonding and thus endows the tellurides with properties and structures which are often totally distinct from those of the sulfides and the selenides.<sup>2</sup> Hence, sulfides and selenides may contain well characterized X<sub>2</sub><sup>2-</sup> pairs of polyanionic X<sub>n</sub><sup>2-</sup> groups with bond lengths of *ca.* 2.05 Å for S and *ca.* 2.35 Å for Se, or non-bonding X<sup>2-</sup>...X<sup>2-</sup> contacts with distances of *ca.* 3.40 Å for S and *ca.* 3.68 Å for Se. In contrast, the tellurides show a wider distribution of Te...Te distances ranging from (Te–Te)<sup>2-</sup> single bond (at around 2.763 Å for instance in HfTe<sub>5</sub>), intermediate Te...Te distances of 3.455(1) Å in NiTe<sub>2</sub>,<sup>3</sup> 3.497(2) Å in IrTe<sub>2</sub>,<sup>4</sup> and non-bonding Te<sup>2-</sup>...Te<sup>2-</sup> van der Waals contacts as in HfTe<sub>2</sub> at around 4.0 Å.

From an electronic point of view, tellurium has the top of its sp band at higher energy than that of sulfur and selenium, leading to a more covalent metal–chalcogen bonding and to a lower oxidizing power. Thus, the top portion of the sp-block band may overlap significantly with the bottom portion of the metal d-block band, thereby causing a substantial electron transfer from the sp- to the d-block band.<sup>5,6</sup> This is what happens in many transition-metal ditellurides and is reflected in intertellurium short bonding contacts.<sup>2</sup> Since the highest anti-bonding levels of the anionic band are depopulated, the Te–Te distances within layers and/or between them become shorter because of smaller repulsion (or larger bonding). In some cases, the formation of these Te...Te short bonding contacts may lead to the polymerization of the tellurium sub-network in relation with the known loss of directionality of the tellurium-p orbitals. It is worth noticing that, due to the depletion of the sp anionic band, these materials are expected to present a p-type metallic conduction. Indeed, the sp → d transfer corresponds to a partial oxidation of the telluride ions with the occurrence of fractional oxidation states between -II and -I.

This is, of course, a marked difference from the sulfides and selenides.

So far, the Te...Te bonding interactions have been detected from the analysis of crystallographic data and transport measurements and confirmed by band-structure calculations. Tellurium-125 solid-state NMR spectroscopy is a sensitive tool to monitor the oxidation state of tellurium, *i.e.* the extent of the p–d band overlap; <sup>125</sup>Te is a spin  $\frac{1}{2}$  nucleus with a receptivity of *ca.* 12.5 times that of <sup>13</sup>C, a natural abundance of 7% and a very large chemical shift range. The aim of the present paper is to provide some insight into the dynamic aspects of the charge transfer in transition-metal tellurides and to support the geometric and physical considerations with solid-state NMR spectroscopy.

## Features of the <sup>125</sup>Te NMR Spectra

There are two anisotropic contributions to the <sup>125</sup>Te NMR shifts of the transition-metal tellurides: (i) the chemical shift (CS) which arises due to the magnetic shielding produced by the bonding electrons surrounding a given tellurium nucleus, and (ii) the Knight shift (KS), observed with conducting samples and due to the hyperfine interaction between the tellurium nuclei and the delocalized electrons. The CS range of a given nucleus results from the modifications in bond properties. According to Ramsey<sup>7</sup> and Saïka and Slichter,<sup>8</sup> CS may be expressed as the sum of a diamagnetic and a paramagnetic term. Jameson and Gutowsky<sup>9</sup> have shown that, for all nuclei except hydrogen, changes in bond properties have a negligible effect on the diamagnetic term while the paramagnetic term [equation (1)] is strongly affected and thus dominates the CS

$$\sigma^p \propto \frac{1}{\Delta} \left( \langle \frac{1}{r^3} \rangle_p P_u + \langle \frac{1}{r^3} \rangle_d D_u \right) \quad (1)$$

trends where  $\Delta$  is an average energy between valence and excited states,  $\langle 1/r^3 \rangle_{p,d}$  is the mean value of  $r^{-3}$  for outer p or d orbitals of the atom in question, and  $P_u$  and  $D_u$  represent the unbalance of valence electrons in the p or d orbitals. Owing to this multiplicity of parameters one must be cautious when trying to rationalize CS variations even among chemically related compounds. Therefore, we shall restrict our discussion to an empirical level.

<sup>†</sup> Non-SI unit employed: eV ≈ 1.60 × 10<sup>-19</sup> J.

**Table 1** General data and information on transition-metal ditellurides

Compound	Structural type	Number of Tellurium sites <sup>a</sup>	Expected tellurium oxidation state	Shortest Te $\cdots$ Te distances (Å) <sup>b</sup>
HfTe <sub>2</sub>	Pure CdI <sub>2</sub>	1	-2	3.949–4.032
ZrTe <sub>2</sub>	Pure CdI <sub>2</sub>	1	$\approx$ -2	3.950–4.025
TiTe <sub>2</sub>	Polymeric CdI <sub>2</sub>	1 <sup>c</sup>	-1.8	3.757–3.913
TaTe <sub>2</sub>	TaTe <sub>2</sub>	3	$\approx$ -1.8	3.558–3.998
NbTe <sub>2</sub>	TaTe <sub>2</sub>	3	$\approx$ -1.8	3.530–3.988
VTe <sub>2</sub>	TaTe <sub>2</sub>	3 <sup>d</sup>	-1.8	3.447–3.947
WTe <sub>2</sub>	WTe <sub>2</sub>	4	-2	3.496–4.013
IrTe <sub>2</sub>	Polymeric CdI <sub>2</sub>	1	-1.5	3.498–3.928
Rh <sub>1.15</sub> Te <sub>2</sub>	Polymeric CdI <sub>2</sub>	1 <sup>d</sup>	-1.725	3.527–3.609
PtTe <sub>2</sub>	Polymeric CdI <sub>2</sub>	1	-1	3.464–4.025
PdTe <sub>2</sub>	Polymeric CdI <sub>2</sub>	1	-1	3.487–4.036

<sup>a</sup> Number of crystallographic sites per cell. <sup>b</sup> Including intra- and inter-layer distances. <sup>c</sup> Occurrence of mixed-valence Ti<sup>III</sup>/Ti<sup>IV</sup>. <sup>d</sup> Presence of extra cations in the van der Waals gap of Rh<sub>1.15</sub>Te<sub>2</sub>,<sup>12</sup> and possibly in VTe<sub>2</sub>.<sup>13</sup>

The KS arises due to the Pauli paramagnetism of the conduction electrons and usually shifts the resonance lines to high frequency.<sup>10</sup> Since in our samples the electrons at the Fermi level have a high degree of p character there are several possible contributions to the KS.<sup>11</sup> The electrons having s character are responsible for the direct contact interaction. In addition, core-polarization contributions may arise from s and p electrons and p-orbital contributions. However, owing to the large s-electron hyperfine coupling, the KS is dominated by the contact interaction. Hence, the isotropic part of KS can be written as in equation (2). The first factor is the probability density at the

$$\text{KS} \propto \langle |\Psi(0)|^2 \rangle_{E_F} N(E_F) \quad (2)$$

nucleus averaged over the Fermi surface while  $N(E_F)$  is the density of states at the Fermi level. Thus, the KS yields information about the local density of states at the Fermi level for a particular tellurium site. The anisotropic part of KS is due to the dipolar interaction between the tellurium nucleus and the Fermi electrons. The magnitude of this zero-trace anisotropic term depends on the non-s part of the wavefunction at the Fermi level. The KS anisotropy vanishes for sites of cubic symmetry. In powders, the KS interaction usually shifts and broadens the NMR lines. Thus, in transition-metal tellurides the CS is related with the formal ionization degree of the tellurium atom while the KS depends on the density of states at the Fermi level which contains an important tellurium atomic contribution. We can then expect a direct relationship between the <sup>125</sup>Te NMR shift and the tellurium oxidation states.

Since there is very little information in the literature on <sup>125</sup>Te solid-state NMR spectroscopy, we have started by studying some commercially available compounds containing tellurium in a range of oxidation states, *viz.* Te(OH)<sub>6</sub>, TeCl<sub>4</sub>, TeO<sub>2</sub> and elemental tellurium. The results obtained complement the existing tellurium chemical shift data base. Representative members of the transition-metal ditelluride family were then studied.

## Structural Description and Tellurium Oxidation States

All the ditellurides of the transition elements studied here crystallize in a CdI<sub>2</sub>-type structure based on a hexagonal closed packing of anions with every second layer of octahedral sites occupied by the cations. In contrast with their sulfur and selenium analogues, the tellurides often display interacting MTe<sub>2</sub> slabs (see above) with the disappearance of the van der Waals gap. Inside the CdI<sub>2</sub> family it is, thus, necessary to distinguish the true CdI<sub>2</sub>-type structure, with a well identified van der Waals gap, from the so-called 'polymeric CdI<sub>2</sub>-type' structure with no gap and with the tellurium anions linked in the three directions of space. A summary of the structural data is given in Table 1 and a projection of the structures is displayed in Fig. 1.

Among Group 4 ditellurides, only ZrTe<sub>2</sub> and HfTe<sub>2</sub> present a true CdI<sub>2</sub>-type structure with well separated slabs [Fig. 1(a)]. According to Klipstein *et al.*,<sup>14</sup> HfTe<sub>2</sub> exhibits semimetallic properties. This behaviour arises from a small overlap of the tellurium p valence band and the metal d conduction band (about 0.3 eV) and implies a very weak or negligible Te to Hf charge transfer. Thus, its charge balance can be written as Hf<sup>IV</sup>(Te<sup>-II</sup>)<sub>2</sub> and this phase will be used as a Te<sup>-II</sup> reference. Since ZrTe<sub>2</sub> is located between two semimetallic compounds, TiTe<sub>2</sub> and HfTe<sub>2</sub>, it is expected to be also a semimetal. With an electronegativity larger than Hf, ZrTe<sub>2</sub> is supposed to present a larger anion–cation band overlap with a weak electron transfer leading to the Zr<sup>(4-ε)+</sup>(Te<sup>-2+(ε/2)</sup>)<sub>2</sub> charge balance with ε almost zero. In contrast with the two above phases, TiTe<sub>2</sub> is a CdI<sub>2</sub>-polymeric structure with an interslab Te–Te distance of 3.775 Å. From band-structure calculations<sup>5</sup> a mixed-valence Ti<sup>III</sup>/Ti<sup>IV</sup> was inferred, explaining the metallic properties of the material and the X-ray photoelectron spectroscopy (XPS) absorption results at the tellurium threshold.<sup>15</sup> According to ref. 5, 0.4 is transferred to each titanium atom leading to the formal charge balance Ti<sup>3.6+</sup>Te<sup>-1.8</sup><sub>2</sub>.

The Group 5 ditellurides (M = V, Nb or Ta) present metal ions clustered into 'ribbon-chains'. The structures can be described as a monoclinic distortion of the CdI<sub>2</sub>-structure type. The metals distort the MX<sub>2</sub> layers to form the triple M–M bonds shown in Fig. 1(b). Three non-equivalent tellurium crystallographic sites in distinct chemical environments are present. In the three compounds some sizeable p(Te)  $\longrightarrow$  d(M) electron transfer is expected. Calculations performed on VTe<sub>2</sub> indicate the occurrence of Te<sup>-1.8</sup> ions with a d-electron count of about 4/3 on the vanadium cation.<sup>5,6</sup>

The Group 6 metal ions of the MX<sub>2</sub> phases (M = Mo or W) with a d<sup>2</sup> electron count show 'zigzag chains' [Fig. 1(c)]. Band electronic studies indicate that the extent of the p(Te)  $\longrightarrow$  d(M) transfer cannot be large due to the high initial d-electron count. The ionization degree of Te in these materials should thus be similar to that observed in HfTe<sub>2</sub>, *i.e.* with the charge balance W<sup>IV</sup>Te<sup>-II</sup><sub>2</sub>.

The structures of Group 9 and 10 ditellurides are CdI<sub>2</sub>-polymeric [Fig. 1(d)]. In the case of rhodium, the 1:2 stoichiometry cannot be reached under normal experimental conditions and the extra cations (the so-called 'disordered cations') reside between the MTe<sub>2</sub> layers.<sup>12</sup> The composition Rh<sub>1+x</sub>Te<sub>2</sub> (x = 0.15) is the rhodium-poorer of the continuous series of subtractive NiAs-type solid solution. The large p(Te)  $\longrightarrow$  d(M) electron transfer corresponds to the charge balance Rh<sup>III</sup><sub>1.15</sub>(Te<sup>-1.71</sup>)<sub>2</sub> and Ir<sup>III</sup>(Te<sup>-1.5</sup>)<sub>2</sub>. Concerning the Group 10 elements, the M<sup>II</sup>Te<sup>-1</sup><sub>2</sub> charge balance seems to be appropriate. Indeed, as shown from XPS measurements and predicted from the electronic structure calculations made on PdTe<sub>2</sub>, PtTe<sub>2</sub> and NiTe<sub>2</sub>,<sup>3</sup> the transfer is enhanced in the case of the Group 10 phases as compared to the Group 9 compounds.

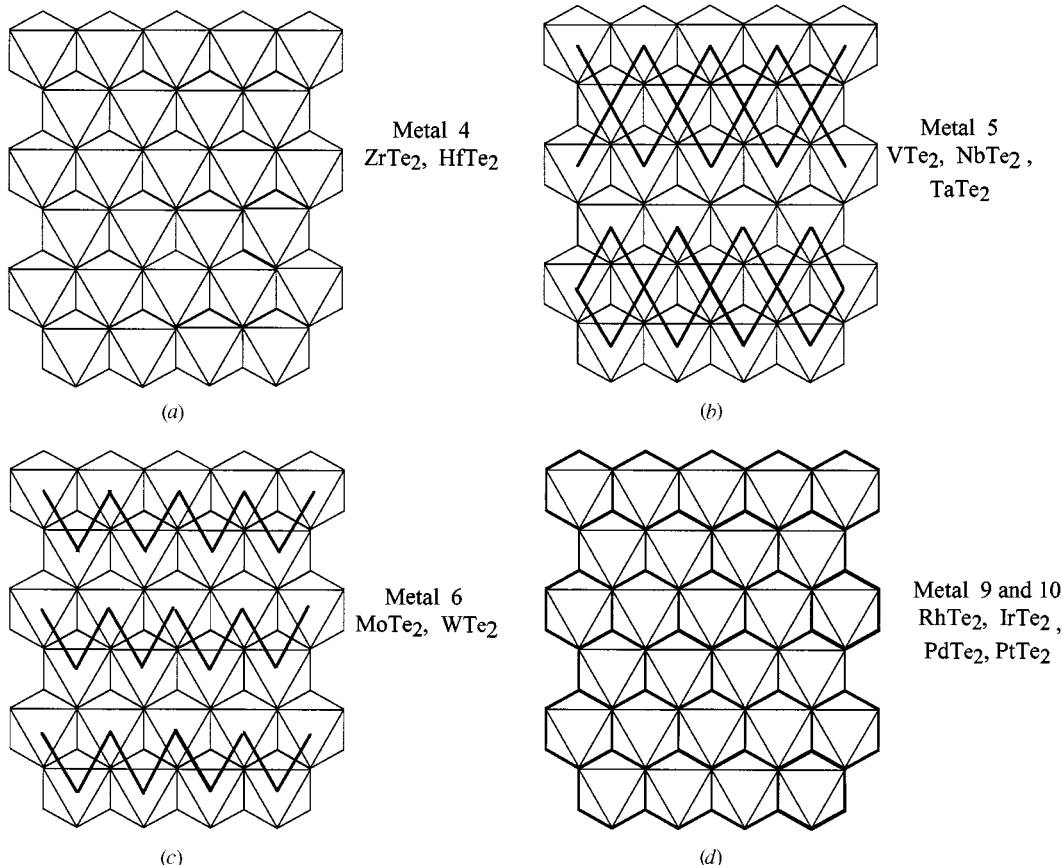


**Fig. 1** Distortion of the CdI<sub>2</sub>-like structure according to the metal group. A projection along the anionic stacking axis is given. Only the Te<sub>6</sub> octahedra are shown. (a) Pure CdI<sub>2</sub>-like structure. (b) A NbTe<sub>2</sub>-like structure with double metal–metal zigzag chains. (c) A WTe<sub>2</sub>-like structure with single metal–metal zigzag chains. (d) Polymeric CdI<sub>2</sub>-like structure with Te–Te bonding interactions (thick lines correspond to these extensive bonds)

**Table 2** Summary of the transition-metal telluride synthesis conditions used

Phase	Synthesis conditions	Parameters (Å and °)
TiTe <sub>2</sub>	950 °C for 190 h, cooled at 5 °C h <sup>-1</sup> to 400 °C, 400 °C for 1 h, cooled at 100 °C h <sup>-1</sup>	$a = 3.7783(6)$ , $c = 6.4828(3)$ , $cla = 1.716$
ZrTe <sub>2</sub>	800 °C for 10 d, quenched in air	$a = 3.9508(2)$ , $c = 6.6256(4)$ , $cla = 1.677$
HfTe <sub>2</sub>	650 °C for 7 d, cooled at 15 °C h <sup>-1</sup>	$a = 3.9497(3)$ , $c = 6.6548(6)$ , $cla = 1.685$
VT <sub>2</sub>	650 °C for 7 d, cooled at 15 °C h <sup>-1</sup>	$a = 19.031(4)$ , $b = 3.6094(7)$ , $c = 9.072(2)$ , $\beta = 134.728(8)$
NbTe <sub>2</sub>	700 °C for 24 h, cooled at 100 °C then 1000 °C for 100 h, cooled at 100 °C h <sup>-1</sup>	$a = 19.666(2)$ , $b = 6.399(4)$ , $c = 9.3199(8)$ , $\beta = 134.638(3)$
TaTe <sub>2</sub>	700 °C for 24 h, cooled at 100 °C h <sup>-1</sup> , 1000 °C for 100 h, cooled at 100 °C h <sup>-1</sup>	$a = 19.258(2)$ , $b = 3.6379(4)$ , $c = 9.3482(7)$ , $\beta = 134.78(4)$
WTe <sub>2</sub>	750 °C for 4 d, cooled at 10 °C h <sup>-1</sup>	$a = 3.4861(4)$ , $b = 6.2690(4)$ , $c = 14.0587(7)$
Rh <sub>1.15</sub> Te <sub>2</sub>	1200 °C for 2 d, cooled at 10 °C h <sup>-1</sup>	$a = 3.9321(1)$ , $c = 5.4396(1)$ , $cla = 1.383$
IrTe <sub>2</sub>	950 °C for 6 h, cooled at 100 °C h <sup>-1</sup> , 600 °C for 20 h, cooled at 100 °C h <sup>-1</sup>	$a = 3.9302(2)$ , $c = 5.3982(3)$ , $cla = 1.374$
PdTe <sub>2</sub>	825 °C for 30 d, cooled at 10 °C h <sup>-1</sup>	$a = 4.0356(4)$ , $c = 5.1313(5)$ , $cla = 1.272$
PtTe <sub>2</sub>	825 °C for 30 d, cooled at 2 °C h <sup>-1</sup>	$a = 4.0273(3)$ , $c = 5.2212(6)$ , $cla = 1.296$

## Experimental

### Sample preparation

Telluric acid, Te(OH)<sub>6</sub>, tellurium tetrachloride, TeCl<sub>4</sub>, tellurium oxide, TeO<sub>2</sub>, and elemental tellurium (99.99%) were from Aldrich. Transition-metal ditellurides and ternary tellurides were prepared by direct combination of the elements taken in stoichiometric amounts. The air-sensitive powders were weighed in a dry-box under nitrogen. The evacuated silica tubes containing the elements were sealed and then heated between 700 and 1000 °C. The synthesis conditions are summarized in Table 2. The purity of the samples was systematically checked by recording the X-ray pattern on a CPS 120 INEL X-ray powder diffractometer using monochromatized radiation (Cu-K $\alpha$ 1 = 1.540 598 Å) or a Siemens D5000 diffractometer in reflection geometry without a monochromator (Cu-K $\alpha$ 1 = 1.540 598, Cu-K $\alpha$ 2 = 1.544 390 Å). The air-sensitive powders were sealed in

a 0.2 mm glass capillary. The results, shown in Table 2, are in agreement with literature data. After ensuring a satisfactory purity of the phases, the samples were studied by NMR spectroscopy. Since ZrTe<sub>2</sub> and VTe<sub>2</sub> are extremely air sensitive, they were kept sealed under vacuum in glass tubes.

### NMR measurements

The <sup>125</sup>Te NMR spectra were recorded at 126.33 MHz on a Bruker MSL-400 P spectrometer. Static experiments were carried out using a standard broad-band Bruker probe. Magic angle spinning (MAS) spectra were measured using a Bruker double-bearing probe. The 4 mm zirconia rotors were spun at rates up to 15 kHz. Two types of experiments were carried out. Single-pulse (Bloch decay) spectra were recorded with 1  $\mu$ s (equivalent to ca. 30°) radiofrequency pulses. In order to avoid the loss of a significant part of the free induction decay (FID) signal during the probe dead-time we have also used Hahn-echo

**Table 3** Tellurium-125 NMR chemical shift parameters for some commercial tellurium compounds

Compound	Number of tellurium sites <sup>a</sup>	$\delta_{\text{iso}}^b$	$\Delta/\text{ppm}$	$\eta$	$\delta_1$	$\delta_2$	$\delta_3$
$\text{Te(OH)}_6$	1	-18.9	87	0.45	-55	-33	32
	2	-25.6	120	0.6	-79	-39	41
$\text{TeCl}_4$	1	1195	-660	0.0	1422	1401	762
	2	1170	-670	0.1	1408	1365	738
$\text{TeO}_2$		749.8	-1295	0.67	1339	866	44
Te		292	-1790	0.0	889	889	-901

<sup>a</sup> Two crystallographic sites per cell in  $\text{Te(OH)}_6$  and in  $\text{TeCl}_4$ . <sup>b</sup> To high frequency of the resonance for  $\text{Te(OH)}_6$  in solution.

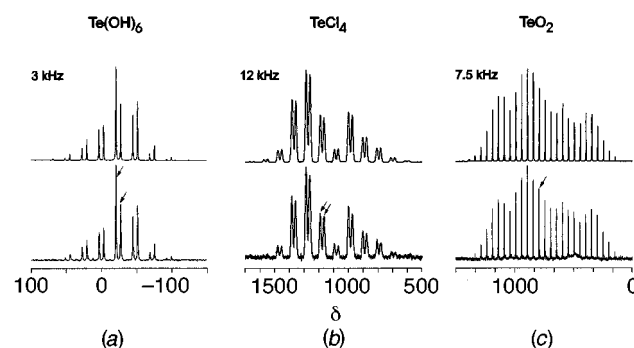


**Fig. 2** Experimental (bottom) and simulated (top)  $^{125}\text{Te}$  NMR MAS spectra of  $\text{Te(OH)}_6$ ,  $\text{TeCl}_4$ , and  $\text{TeO}_2$  recorded at the spinning rates indicated. The arrows depict the isotropic lines

sequences<sup>16</sup> ( $90^\circ-\tau_1-90^\circ-\tau_2$ -acquisition) with  $\tau_1, \tau_2 = 10 \mu\text{s}$ . The recycle delays ranged from 500 ms to 10 s. Owing to the very large  $^{125}\text{Te}$  anisotropies (up to 1500 ppm) usually observed, 10 000 to 50 000 transients were recorded for each sample. In addition, MAS rates above 12 kHz must be used. The conducting samples were ground and dispersed in an insulating and inert  $\text{ZrO}_2$  powder. This dispersion lowered somewhat the effective sensitivity but it ensured a better penetration of the radiofrequency fields and improved the probe tuning *via* modification of the dielectric properties. On the other hand, lowering the sample density made it possible to spin the rotors faster. Shifts are quoted in ppm from saturated aqueous  $\text{Te(OH)}_6$ .<sup>17</sup>

For conducting samples, the Korringa relation predicts that the spin-lattice relaxation time  $T_1$  varies as a function of  $1/T$ . Owing to the very long times required to record a single  $^{125}\text{Te}$  NMR spectrum it is not feasible to measure  $T_1$  at several different temperatures. Consequently, we shall turn to more qualitative arguments to confirm that KS contributes significantly to the  $^{125}\text{Te}$  shifts observed for many of our samples.

In order to extract parameters characterizing line shifts and anisotropies the MAS and static NMR spectra were simulated using the computer program QUASAR.<sup>18</sup> In the case of transition-metal ditellurides we did not attempt to simulate the spectra considering two different tensors (CS and KS). Rather, we have only tried to simulate the spectra of samples for which the pattern is characteristic of a single tensorial interaction. The principal components of the tensor ( $\delta_{ii}$ ) are labelled according to the convention  $|\delta_{33} - \delta_{\text{iso}}| > |\delta_{11} - \delta_{\text{iso}}| > |\delta_{22} - \delta_{\text{iso}}|$ , where  $\delta_{\text{iso}}$  is the isotropic shift (positive to high frequency). The anisotropy  $\Delta = \delta_{33} - \delta_{11}$  may be positive or negative. The asymmetry parameter is  $\eta = (\delta_{22} - \delta_{11})/(\delta_{33} - \delta_{\text{iso}})$ .

## Results and Discussion

### Commercially available tellurium compounds

**Tellurium-(IV) and -(VI) inorganic salts.** Fig. 2 shows experimental and simulated MAS spectra of  $\text{Te(OH)}_6$ ,  $\text{TeCl}_4$  and  $\text{TeO}_2$ . For each sample at least three different spinning rates were used. In all cases good fittings were obtained and the extracted tensor information is collected in Table 3. For

$\text{Te(OH)}_6$  we have measured  $^1\text{H}-^{125}\text{Te}$  cross-polarization MAS spectra and obtained results similar to those reported by Collins and Ripmeester<sup>17</sup> [Fig. 2(a)].  $\text{TeCl}_4$  has not yet been studied by solid-state NMR spectroscopy. The spectrum shown in Fig. 2(b) clearly contains two resonances at  $\delta$  1170 and 1195 in a 1:1 intensity ratio. Their similar shielding tensors are characterized by a large negative anisotropy ( $|\Delta| \text{ ca. } 660-670 \text{ ppm}$ ) and an almost axial symmetry. These results are consistent with the local symmetry around the two crystallographic tellurium sites.<sup>19</sup> Each tellurium has three chlorine atoms as first neighbours which form an equilateral trigonal pyramid with an average Te-Cl distance of 2.311 Å. Three bridging Cl atoms with much longer Te-Cl distances (average 2.929 Å) complete the tellurium co-ordination sphere producing a strongly distorted octahedron. The axial symmetry of the CS tensor may be related to the  $C_{3v}$  symmetry axis of the  $\text{TeCl}_3^+$  units. The isotropic CS values obtained from solution are strongly dependent on the solvent. For example,  $\text{TeCl}_4$  resonates at  $\delta$  426 in  $\text{Me}_2\text{CO}$  and at  $\delta$  1013 in tetrahydrofuran [relative to  $\text{Te(OH)}_6$ ].<sup>20</sup> Tellurium dioxide gives a single  $^{125}\text{Te}$  resonance [Fig. 2(c)]. All tellurium atoms are crystallographically equivalent and the general, very large CS anisotropy (-1295 ppm) is consistent with the reported structure.<sup>21,22</sup> The solid contains square-pyramidal ( $\text{TeO}_4$ ) units with Te at the apex. There are two short and two long Te-O bonds (1.91 and 2.09 Å respectively).

**Elemental tellurium.** Elemental tellurium is on the borderline between metals and non-metals. This narrow-gap (0.33 eV) semiconductor displays a crystalline hexagonal lattice made of spiral chains of tellurium.<sup>23</sup> Fig. 3 shows experimental and simulated MAS and static NMR spectra. In elemental tellurium all sites are equivalent. The CS tensor displays a negative sign and is axially symmetric. The value we found for the anisotropy ( $|\Delta| \text{ ca. } 1790 \text{ ppm}$ ) is slightly smaller than that obtained by Bensoussan<sup>24</sup> from single-crystal studies ( $|\Delta| \text{ ca. } 1866 \text{ ppm}$ ).

### MTe<sub>2</sub> binary phases

Fig. 4 displays static  $^{125}\text{Te}$  NMR spectra of binary compounds. For the spectra which have been simulated from both static and MAS experiments, the principal elements characterizing the tensor interaction are reported in Table 4. For the other cases only approximate averaged isotropic shifts (first moment of the static line) and total anisotropy widths ( $\Delta$ ) are given. We shall first comment on the individual static NMR lines following the order of the metal element groups.

**HfTe<sub>2</sub>, ZrTe<sub>2</sub> and TiTe<sub>2</sub> (Group 4).** The static line shapes of  $\text{HfTe}_2$  and  $\text{ZrTe}_2$  indicate the presence of a single tellurium site characterized by an axially symmetric tensor. Indeed, one unique site is expected in the  $\text{CdI}_2$ -type structure displayed by these compounds: the tellurium atoms are on the  $C_3$  symmetry axis of an hexagonal lattice. Since these compounds present a negligible or weak sp → d electron transfer, one may assume that the shape of the resonance lines is dominated by the CS interaction. Hence, the axial symmetry of the shielding tensor is determined by the crystal symmetry. Since for these samples the

**Table 4** Tellurium-125 NMR shifts and anisotropy parameters for transition-metal tellurides

Compound	Number of tellurium sites <sup>a</sup>	$\delta_{\text{iso}}^b$	$\Delta^c/\text{ppm}$	$\eta$	$\delta_1$	$\delta_2$	$\delta_3$
WTe <sub>2</sub>	4	550–600	600–900	—	—	—	—
HfTe <sub>2</sub>	1	920	890	0	623	623	1513
ZrTe <sub>2</sub>	1	≈1825	750–800	0	—	—	—
TaTe <sub>2</sub>	3	≈2600	800–1000	—	—	—	—
NbTe <sub>2</sub>	3	≈3300	≈600	—	—	—	—
VTe <sub>2</sub>	3	3400–3600	1500–2000	—	—	—	—
TiTe <sub>2</sub>	1	≈3800	≈900	—	—	—	—
Rh <sub>1.15</sub> Te <sub>2</sub>	1	≈4300	≈1500	—	—	—	—
IrTe <sub>2</sub>	1	4750	135	0	4705	4705	4840
PdTe <sub>2</sub>	1	5510	460	0	5355	5355	5815
PtTe <sub>2</sub>	1	≈7400	1000–1500	—	—	—	—

<sup>a</sup> Number of crystallographic sites per cell. <sup>b</sup> To high frequency of resonance for Te(OH)<sub>6</sub> in solution. <sup>c</sup>  $\Delta$  is the total spectral width of the static line.

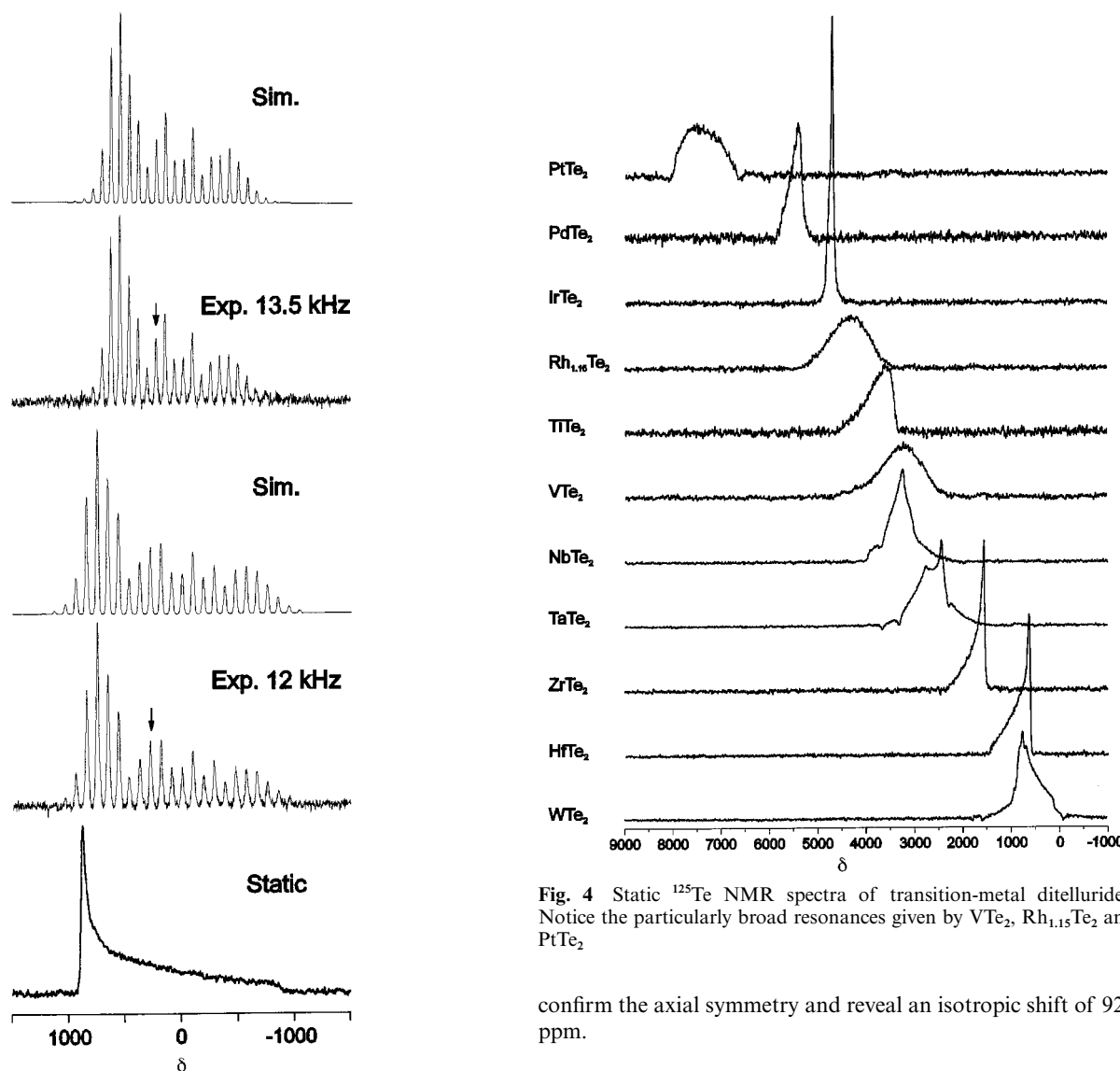


**Fig. 3** Experimental and simulated  $^{125}\text{Te}$  static and MAS NMR spectra of elemental tellurium recorded at the spinning rates indicated. The arrows indicate the isotropic lines

tensors are positive, it is fair to assume that the less shielded principle axis lies along  $C_3$ . The line shape is somewhat different for TiTe<sub>2</sub> due to a significant broadening. The mixed-valence Ti<sup>III</sup>/Ti<sup>IV</sup> (in a 2:3 atomic ratio) expected for this compound<sup>5</sup> generates a distribution in tellurium environments which contributes to the observed broadening. The NMR spectrum of HfTe<sub>2</sub> has also been studied at several MAS rates. The experimental and simulated spectra recorded at 12 kHz [Fig. 5(a)]

**Fig. 4** Static  $^{125}\text{Te}$  NMR spectra of transition-metal ditellurides. Notice the particularly broad resonances given by VTe<sub>2</sub>, Rh<sub>1.15</sub>Te<sub>2</sub> and PtTe<sub>2</sub>

confirm the axial symmetry and reveal an isotropic shift of 920 ppm.

**VTe<sub>2</sub>, NbTe<sub>2</sub>, TaTe<sub>2</sub> (Group 5) and WTe<sub>2</sub> (Group 6).** The static  $^{125}\text{Te}$  NMR lines of WTe<sub>2</sub>, TaTe<sub>2</sub> and NbTe<sub>2</sub> display several singularities suggesting that different spectral lines overlap. The structures contain four, three and three crystallographically inequivalent tellurium sites, respectively. Owing to the presence of several overlapping lines it was not possible to simulate the static spectra. We have, thus, resorted to MAS studies, but even when the highest spinning rate available (15 kHz) was used the spectra displayed a very large number of overlapping spinning sideband patterns preventing simulation. Hence, the isotropic shifts given in Table 4 are the approximate centres of gravity of the spectral lines. The static  $^{125}\text{Te}$  NMR spectrum of VTe<sub>2</sub>

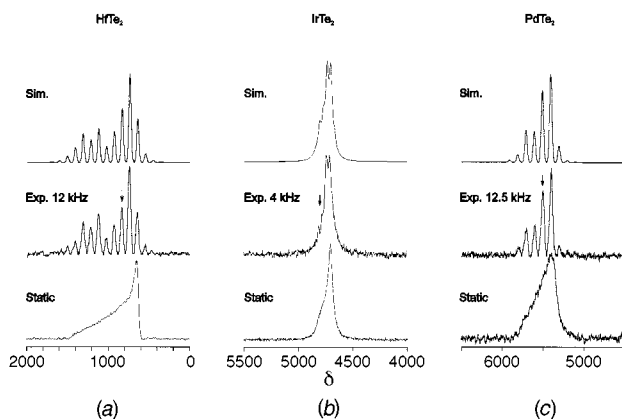


**Fig. 5** Experimental and simulated static and MAS  $^{125}\text{Te}$  NMR spectra of  $\text{HfTe}_2$ ,  $\text{IrTe}_2$  and  $\text{PdTe}_2$  recorded at the spinning rates indicated. The arrows depict the isotropic lines

(three inequivalent tellurium sites) is considerably broadened in comparison with those of the other members of Group 5. Depending on the synthesis conditions,<sup>13</sup> the possible presence of extra cations in the van der Waals gap may generate a distribution in the tellurium surroundings. This may contribute to the observed line broadening.

**IrTe<sub>2</sub> and Rh<sub>1.15</sub>Te<sub>2</sub> (Group 9).** The compound IrTe<sub>2</sub> contains a single tellurium crystallographic site and has the smallest anisotropy ( $\Delta$  ca. 150 ppm) of all the tellurides studied. Experimental and simulated spectra [Fig. 5(b)] indicate that besides shift anisotropy there is another source of line broadening. Indeed, the usual singularity on the high-frequency side ( $\Delta > 0$ ) of the static spectrum is poorly defined. The Rh<sub>1.15</sub>Te<sub>2</sub> static spectrum exhibits an extremely broad nearly gaussian line. In this compound the 0.15 additional rhodium atom partially fills the van der Waals gap of the polymeric-CdI<sub>2</sub> lattice<sup>12</sup> leading to different tellurium chemical environments, and this explains the line broadening.

**PdTe<sub>2</sub> and PtTe<sub>2</sub> (Group 10).** The compound PdTe<sub>2</sub> contains a single tellurium site and gives a resonance characteristic of an axially symmetric shift tensor [Fig. 5(c)]. Clearly, other sources of line broadening operate. The compound PtTe<sub>2</sub> gives an extremely broad static line ( $\Delta$  ca. 1300 ppm) which is of the order of the spectral width observed for VTe<sub>2</sub> and Rh<sub>1.15</sub>Te<sub>2</sub>. However, since the PtTe<sub>2</sub> polymeric-CdI<sub>2</sub> structure contains a single tellurium site, the broadening is not due to a distribution of sites (in contrast with TiTe<sub>2</sub>, VTe<sub>2</sub> and Rh<sub>1.15</sub>Te<sub>2</sub>) and this will be discussed later.

#### $^{125}\text{Te}$ NMR shift range for tellurium compounds

Fig. 6 summarizes all the available information on solid-state  $^{125}\text{Te}$  NMR shifts for various types of tellurium-containing compounds. Notice that the transition-metal ditellurides appear on the high-frequency side of the scale. This is strong evidence that a significant paramagnetic KS occurs for these compounds, while for non-conducting materials the CS range extends from  $\delta$  ca. -2000 to 1000 ppm. A preliminary study of Nb<sub>2</sub>SiTe<sub>4</sub>, Nb<sub>3</sub>SiTe<sub>6</sub> and Nb<sub>3</sub>GeTe<sub>6</sub> has shown that binary and ternary tellurides give resonances in the same high-frequency range.<sup>25</sup> Semiconducting MTe compounds ( $M = \text{Hg, Zn, Cd, Pb or Sn}$ ) have been studied previously by solid-state NMR spectroscopy.<sup>26-29</sup> At room temperature the  $^{125}\text{Te}$  shifts range from  $\delta$  -1600 to -1900 ppm in the undoped state. Data on organotellurium compounds are derived from solution studies and they range from  $\delta$  -1920 to 530 ppm.<sup>17,20,30-32</sup> Organometal-tellurium complexes resonate in the same region ( $\delta$  -2000 to 410 ppm).<sup>33</sup> Tellurium salts with various positive tellurium oxidation states yield a range from  $\delta$  -2140 to 1250 ppm.<sup>20,34-36</sup> On the whole,  $^{125}\text{Te}$  shifts cover a remarkably large

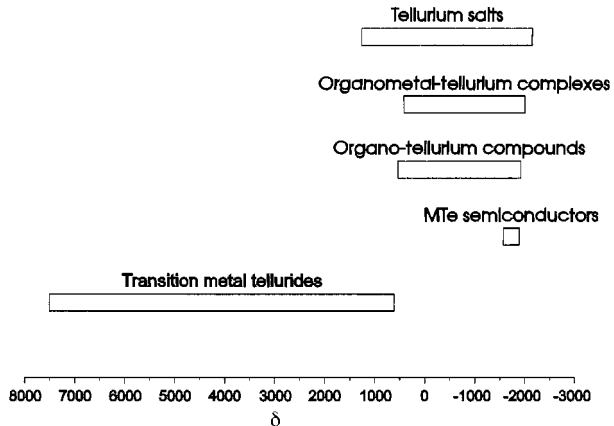


**Fig. 6** The  $^{125}\text{Te}$  NMR shift ranges [referred to aqueous  $\text{Te}(\text{OH})_6$ ] for tellurium compounds: transition-metal ditellurides and ternary tellurides,<sup>25</sup> MTe semiconductors,<sup>26-29</sup> organotellurium compounds,<sup>17,20,30-32</sup> organometal-tellurium complexes,<sup>33</sup> and tellurium salts (including our results and refs. 20, 34-36)

range of ca. 10 000 ppm. Large CS ranges are usually observed with high atomic number magnetic nuclei ( $Z = 52$  for tellurium). In general, an increase in the CS ranges occurs periodically along each period or within a group of the Periodic Table. Jameson and Gutowsky<sup>9</sup> have shown that this evolution parallels the trend of  $\langle l/r^3 \rangle_{p,q}$  in equation (1). Since the equation for each principal element of the CS tensor is also proportional to this factor, this may explain the broad tensor widths  $\Delta$  observed in our  $^{125}\text{Te}$  solid-state NMR studies.

#### Sources of line broadening

In addition to a distribution of sites present in some samples ( $\text{TiTe}_2$ ,  $\text{Rh}_{1.15}\text{Te}_2$  and perhaps  $\text{VTe}_2$ ) the possible sources of broadening of the NMR lines given by transition-metal tellurides are of multiple origins. Static linewidths up to 1500–2000 ppm are seen in Fig. 4. Such values are of the order of magnitude of the very large shielding anisotropies we have measured for commercial tellurium-containing compounds (ca. 1300 and 1800 ppm for  $\text{TeO}_2$  and elemental tellurium, respectively). Notice that for conducting tellurides both CS and KS anisotropies contribute to the lineshape. The latter is due to the local field produced by p electrons and may not exceed 10% of the contact interaction (s electrons) which produces the Knight shift.<sup>37</sup> However the relative importance of CS and KS anisotropies is difficult to evaluate. Their combination may result in a broadening of the powder spectrum when one of the anisotropies dominates, but when both are of the same order complex or atypical line shapes may result. This may in part explain the very broad line shape of  $\text{PtTe}_2$  for which there is no site distribution.

The direct dipolar interaction, partially averaged in MAS experiments, also introduces an extra broadening. This is evidenced by comparing MAS and static spectra because the simulation of the latter generally requires a significantly larger broadening factor. Weak homonuclear dipolar couplings are expected since  $^{125}\text{Te}$  is only 7% abundant. The heteronuclear dipolar  $^{125}\text{Te}$ –M interaction may be significant for samples where M is a magnetic nucleus with  $\gamma_M$  similar to  $\gamma_{\text{Te}}$ . On the other hand, in these crystal structures each tellurium atom has three metal atoms as first neighbours placed at short distances (2.6–2.7 Å). Line broadening due to  $^{125}\text{Te}$ –M dipolar interaction is particularly important for  $^{51}\text{V}$  ( $I = \frac{7}{2}$ ),  $^{93}\text{Nb}$  ( $I = \frac{9}{2}$ ) and  $^{195}\text{Pt}$  ( $I = \frac{1}{2}$ ) which are 100, 100 and 34% abundant, respectively, with Larmor frequencies (105.15, 97.84, 85.99 MHz, respectively) close to that of  $^{125}\text{Te}$  (126.33 MHz). Indirect J couplings may also occur in transition-metal tellurides. This interaction is directly proportional to the product  $\gamma_M \gamma_{\text{Te}}$  and it depends on the natural abundances of the isotopes. Moreover, it depends

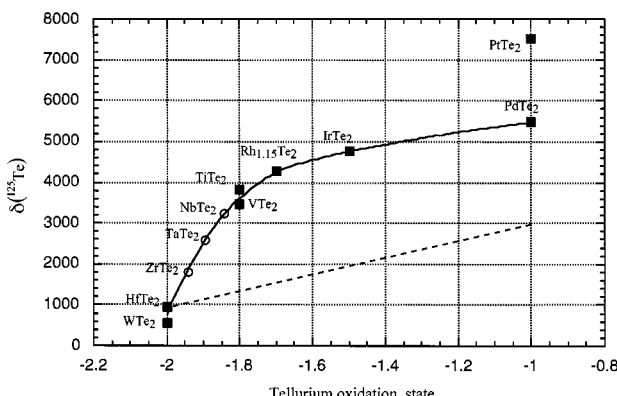


Fig. 7 Plot of the  $^{125}\text{Te}$  NMR shift in transition-metal ditellurides *vs.* tellurium oxidation state: ■, oxidation state calculated from extended-Hückel and physical measurements; ○, interpolated. The dashed line represents the estimated chemical shift contribution (see text)

on the nature and geometry of bonding electrons and on the s character of the bonding orbitals. Owing to the latter, the magnitude of the  $J$  interaction increases periodically with the atomic number of the nuclei involved, in the same way the CS range does. As an example, very large  $^{125}\text{Te}$ – $^{195}\text{Pt}$   $^1J$  couplings (*ca.* 6 kHz) have been reported for  $[(\text{PtCl}_3)_2\text{TeMe}_2]^{2-}$  in solution.<sup>38</sup> In the solid state,  $^{125}\text{Te}$ – $^{199}\text{Hg}$  anisotropic  $J$  couplings of *ca.* 7 kHz have been observed in the static  $^{125}\text{Te}$  NMR spectrum of  $\text{HgTe}$ .<sup>39</sup> Finally, conduction electrons may also be responsible for another type of indirect coupling, for which the theory predicts very long-range effects.<sup>40</sup>

#### Correlation between the $^{125}\text{Te}$ total shift and the tellurium oxidation state

We now discuss the relation between the  $^{125}\text{Te}$  NMR data and the  $\text{sp}(\text{Te}) \longrightarrow \text{d}(\text{M})$  electron transfer in transition-metal binary ditellurides with a  $\text{CdI}_2$ -related structure. In practice, this means attempting to correlate the NMR shift with the tellurium oxidation state (from  $-\text{II}$  to  $-\text{I}$  in our compounds). As far as the CS interaction is concerned, the oxidation of tellurium should result in a progressive paramagnetic shift through a deshielding effect. Also the KS is expected to vary as a function of the characteristics of the Fermi surface of the different compounds.

Fig. 7 shows the relation between  $^{125}\text{Te}$  NMR shifts and tellurium oxidation states. The general trend is an increase of the NMR shift when the tellurium oxidation state increases, ranging from  $\delta$  550 for  $\text{W}^{4+}\text{Te}^{-2}$  to  $\delta$  7400 for  $\text{Pt}^{2+}\text{Te}^{-1}$ . On the low-frequency side, the  $\text{WTe}_2$  and  $\text{HfTe}_2$  resonances are found around  $\delta$  600 and 900. Their oxidation state is close to or exactly  $-\text{II}$ . The relative paramagnetic shift observed from  $\text{HfTe}_2$  to  $\text{ZrTe}_2$  (at *ca.* 900 and 1800 ppm, respectively) is consistent with an increased overlap between the p- and d-block bands. Although the degree of the  $\text{sp}(\text{Te}) \longrightarrow \text{d}(\text{Zr})$  electron transfer in  $\text{ZrTe}_2$  is not known, we can assume that its oxidation state lies between that of  $\text{HfTe}_2$  and  $\text{TiTe}_2$ . From a cubic spline fit (see Fig. 7), a tellurium oxidation state equal to about  $-1.95$  can be estimated for  $\text{ZrTe}_2$ . On the other hand,  $\text{TiTe}_2$  gives a markedly shifted signal at  $\delta$  *ca.* 3800. The large paramagnetic shift between  $\text{ZrTe}_2$  and  $\text{TiTe}_2$  is consistent with the important electron transfer occurring in titanium ditelluride (oxidation state calculated at  $-1.8$ ).

For  $\text{VTe}_2$  calculations have indicated an electron transfer comparable to that in  $\text{TiTe}_2$ .<sup>5,6</sup> Since in these compounds the local environments of tellurium are very similar one expects  $^{125}\text{Te}$  resonances at similar shifts and this is indeed observed ( $\delta$  3400 and 3800 for  $\text{VTe}_2$  and  $\text{TiTe}_2$ , respectively). Among Group 5 transition metals the electronegativity decreases from V (1.63) to Nb (1.60) and Ta (1.50) implying a decrease of the  $\text{sp}(\text{Te}) \longrightarrow \text{d}(\text{M})$  electron transfer from  $\text{VTe}_2$  to  $\text{NbTe}_2$  and

$\text{TaTe}_2$ . In accordance, the  $^{125}\text{Te}$  NMR lines shift from  $\delta$  3400 ( $\text{VTe}_2$ ) to 2600 ( $\text{TaTe}_2$ ). Again, the exact degrees of transfer have not been calculated in  $\text{NbTe}_2$  or  $\text{TaTe}_2$  but they are expected to be between those of  $\text{ZrTe}_2$  and  $\text{VTe}_2$ . Values of  $-1.85$  and  $-1.88$  for the tellurium oxidation state in  $\text{NbTe}_2$  and  $\text{TaTe}_2$ , respectively, are derived from Fig. 7.

Consider now the Group 9 transition-metal ditellurides. For  $\text{IrTe}_2$  a tellurium oxidation state of  $-1.5$  corresponds to a resonance at  $\delta$  4750, clearly deshielded relatively to the tellurium signal of  $\text{TiTe}_2$ . The case of rhodium ditelluride is somewhat different since the stoichiometric material does not exist. The rhodium-poor phase is  $\text{Rh}_{1.15}\text{Te}_2$  and the oxidation state is calculated at  $-1.7$ . Such difference in oxidation state is consistent with the 440 ppm paramagnetic shift observed between  $\text{Rh}_{1.15}\text{Te}_2$  and  $\text{IrTe}_2$ . In  $\text{PtTe}_2$  and  $\text{PdTe}_2$  the oxidation state is expected to be  $-1$  and the compounds display the most deshielded resonances of the series. However their shift difference of almost 2000 ppm is totally unexpected.

Except for  $\text{PtTe}_2$  and  $\text{PdTe}_2$ , the relative shifts of  $^{125}\text{Te}$  NMR lines are in good qualitative agreement with the concept of  $\text{Te} \rightarrow \text{M}$  electron transfer. Further discussion of the NMR results would require the separation of CS and KS contributions. As equation (2) shows, the KS is proportional to the electron density at the Fermi level. Band-structure calculations performed on transition-metal tellurides have shown that the orbitals participating at the Fermi level are essentially anionic.<sup>5,6</sup> Hence the KS should be correlated with the tellurium oxidation state. On the other hand, an order of magnitude for the possible influence of tellurium oxidation state variations on the CS can be estimated from solution studies. For poly-chalcogenide anions in solution Björgvinsson and Schrödabringen<sup>35</sup> have found that the resonance positions of species such as  $\text{Te}^{-\text{II}}_2$ ,  $\text{Te}^{-\text{II}}_3$  and  $\text{Te}^{-\text{II}}_4$  show a relative paramagnetic shift of *ca.* 2000 ppm per electron. Assuming a linear dependence between CS and tellurium oxidation state, the line drawn in Fig. 7 corresponds to the estimated CS contribution for the total NMR shift observed with transition-metal ditellurides. The compounds  $\text{WTe}_2$  and  $\text{HfTe}_2$  which have the smallest electron transfer and thus an oxidation state of  $-\text{II}$  provide a reference for the CS. The distances from each point to the model line give a crude estimation of the KS contribution. For example, a similar order of magnitude (*ca.* 2500 ppm) is obtained for the KS in  $\text{TiTe}_2$ ,  $\text{Rh}_{1.15}\text{Te}_2$ ,  $\text{IrTe}_2$  and  $\text{PdTe}_2$  while the paramagnetic shift of  $\text{PtTe}_2$  must be explained by a significantly larger KS (*ca.* 4500 ppm). Such high  $^{125}\text{Te}$  KS values are consistent with those generally reported for heavy nuclei.<sup>11</sup> In our case, they should be related to the s-electron density on the tellurium nuclei.

#### Conclusion

We have shown that solid-state  $^{125}\text{Te}$  NMR spectroscopy is a sensitive tool to probe the local environment of tellurium in a wide range of compounds. Our study of commercially available tellurium compounds and transition-metal tellurides together with the previously reported work allowed us to build up a NMR shift database on this poorly studied nucleus. The  $^{125}\text{Te}$  NMR shifts cover a large range of *ca.* 10 000 ppm *versus* tellurium chemical environments, oxidation states and electronic properties. The transition-metal tellurides resonate on the high-frequency side of this scale. This observation has been attributed to the KS occurring for these conducting samples. In the transition-metal ditelluride family the total  $^{125}\text{Te}$  NMR shift, including CS and KS, correlates well with the expected tellurium oxidation state: the paramagnetic shift increases with increasing overlap of the anionic sp band and the cationic d levels, providing a tool for the estimation of the  $\text{Te} \rightarrow \text{M}$  electron transfer. Thus the present study, although only semiquantitative, supports the previous electronic band structure calculations which have shown that weak anionic bondings occur.

From the total NMR shift we have attempted to separate the CS from the KS contribution.

Complementary tellurium Mössbauer spectroscopic studies on the same tellurides are in progress. Preliminary results seem to show the same kind of trend in isomer shift *versus* tellurium oxidation state.<sup>41</sup>

## Acknowledgements

This work has been supported by the European Commission under the HCM program CHRX-CT94-0675. We thank Drs J. Conard (Orléans) and E. Canadell (Barcelona) for valuable discussions and suggestions.

## References

- 1 P. Böttcher, *Angew. Chem., Int. Ed. Engl.*, 1988, **27**, 759.
- 2 S. Jobic, R. Brec and J. Rouxel, *J. Alloys Compounds*, 1992, **178**, 253.
- 3 W. Bensch, W. Heid, M. Muhler, S. Jobic, R. Brec and J. Rouxel, *J. Solid State Chem.*, 1996, **121**, 87.
- 4 S. Jobic, P. Deniard, R. Brec and J. Rouxel, *Z. Anorg. Allg. Chem.*, 1991, **598-599**, 199.
- 5 E. Canadell, S. Jobic, R. Brec, J. Rouxel and M.-H. Whangbo, *J. Solid State Chem.*, 1992, **99**, 189.
- 6 M.-H. Whangbo and E. Canadell, *J. Am. Chem. Soc.*, 1992, **114**, 9587.
- 7 N. F. Ramsey, *Phys. Rev.*, 1950, **77**, 567.
- 8 A. Säika and C. P. Slichter, *J. Chem. Phys.*, 1954, **22**, 26.
- 9 C. J. Jameson and H. S. Gutowsky, *J. Chem. Phys.*, 1964, **40**, 1714.
- 10 W. D. Knight, *Solid State Phys.*, 1957, **2**, 92.
- 11 G. C. Carter, L. H. Bennett and D. J. Kahan, in *Metallic shifts in NMR, Progress in Material Science*, Pergamon, Oxford, 1977, vol. 20, part I.
- 12 R. Krachler and H. Ipser, *Z. Metallkd.*, 1996, **87**, 4.
- 13 K. D. Bronsema, G. W. Bus and G. A. Wiegen, *J. Solid State Chem.*, 1984, **53**, 415.
- 14 P. C. Klipstein, D. R. P. Guy, E. A. Marseglia, J. I. Meakin, R. H. Friend and A. D. Yoffe, *J. Phys. C.*, 1986, **19**, 4953.
- 15 Y. Arnaud and M. Chevreton, *J. Solid State Chem.*, 1981, **39**, 230.
- 16 M. Rance and R. A. Byrd, *J. Magn. Reson.*, 1983, **52**, 221.
- 17 M. J. Collins and J. A. Ripmeester, *J. Am. Chem. Soc.*, 1987, **109**, 4113.
- 18 J. P. Amoureaux, C. Fernandez, L. Carpentier and E. Cochon, *Phys. Status Solidi A*, 1992, **132**, 462.
- 19 B. Buss and B. Krebs, *Inorg. Chem.*, 1971, **10**, 2795.
- 20 *NMR and the Periodic Table*, eds. R. K. Harris and B. E. Mann, 1978, ch. 12, p. 412.
- 21 J. Leciejewicz, *Z. Kristallogr.*, 1961, **116**, 345.
- 22 W. A. Dutton and W. C. Cooper, *Chem. Rev.*, 1966, **66**, 657.
- 23 C. Adenis, V. Langer and O. Lindqvist, *Acta Crystallogr., Sect. C*, 1989, **45**, 941.
- 24 M. Bensoussan, *J. Phys. Chem. Solids*, 1967, **28**, 1533.
- 25 I. Orion and J. Rocha, unpublished work.
- 26 A. Willig, B. Sapoval, K. Leibler and C. Vérité, *J. Phys. C: Solid State Phys.*, 1976, **9**, 1981.
- 27 A. Willig and B. Sapoval, *J. Phys. Lett.*, 1977, **38**, L-57.
- 28 W. Koch, O. Lutz and A. Nolle, *Z. Phys. A*, 1978, **289**, 17.
- 29 B. Perrin and F. T. Hedgcock, *J. Phys. C: Solid State Phys.*, 1982, **15**, 6307.
- 30 H. C. E. McFarlane and W. McFarlane, *J. Chem. Soc., Dalton Trans.*, 1973, 2416.
- 31 W. McFarlane, F. J. Berry and B. C. Smith, *J. Org. Chem.*, 1976, **41**, 139.
- 32 H. Duddeck and A. Biallaß, *Magn. Reson. Chem.*, 1994, **32**, 303.
- 33 W. A. Hermann and H. J. Kneuper, *J. Organomet. Chem.*, 1988, **348**, 193.
- 34 M. J. Collins and R. J. Gillespie, *Inorg. Chem.*, 1984, **23**, 1975.
- 35 M. Björgvinnsson and G. J. Schrolbingen, *Inorg. Chem.*, 1991, **30**, 2540.
- 36 R. J. Batchelor, F. W. B. Einstein, I. D. Gay, C. H. W. Jones and R. D. Sharma, *Inorg. Chem.*, 1993, **32**, 4378.
- 37 T. J. Rowland, *Prog. Met. Phys.*, 1961, **9**.
- 38 P. L. Goggin, R. J. Goodfellow and S. R. Haddock, *J. Chem. Soc., Chem. Commun.*, 1975, 176.
- 39 R. Baltz, M. Haller, W. E. Hertler, O. Lutz, A. Nolle and R. Schafitel, *J. Magn. Reson.*, 1980, **40**, 9.
- 40 M. A. Ruderman and C. Kittel, *Phys. Rev.*, 1954, **96**, 99.
- 41 J. N. Durand, J. C. Dumas, V. Abadie, R. Brec, S. Jobic and E. Molins, unpublished work.

Received 4th July 1997; Paper 7/04757F